Preprint typeset using LaTeX style emulateapj v. 10/09/06

COSMIC EVOLUTION OF BLACK HOLES AND SPHEROIDS. II: SCALING RELATIONS AT $Z = 0.36$

Tommaso Treu[1,2], Jong-Hak Woo[1], Matthew A. Malkan[3], Roger D. Blandford[4]

(Received 10 April 2007; Accepted 2 June 2007)

ABSTRACT

We use high resolution images obtained with the Advanced Camera for Surveys on board the Hubble Space Telescope to determine morphology, nuclear luminosity and structural parameters of the spheroidal component for a sample of 20 Seyfert galaxies at $z = 0.36$. We combine these measurements with spectroscopic information from the Keck Telescope (paper I) to determine the black hole mass - spheroid luminosity relation (M_{BH}-L_B), the Fundamental Plane (FP) of the host galaxies and the black hole mass - spheroid velocity dispersion relation (M_{BH}-σ). The FP is consistent with that of inactive spheroids at comparable redshifts. Assuming pure luminosity evolution, we find that the host spheroids had smaller luminosity and stellar velocity dispersion than today for a fixed M_{BH}. The offsets correspond to $\Delta \log L_{B,0} = 0.40 \pm 0.11 \pm 0.15$ ($\Delta \log M_{BH} = 0.51 \pm 0.14 \pm 0.19$) and $\Delta \log \sigma = 0.13 \pm 0.03 \pm 0.05$ ($\Delta \log M_{BH} = 0.54 \pm 0.12 \pm 0.21$), respectively for the M_{BH}-L and M_{BH}-σ relations (the double error bars indicate random and systematic uncertainties). A detailed analysis of known systematic errors and selection effects shows that they cannot account for the observed offset. We conclude that the data are inconsistent with pure luminosity evolution and the existence of universal and tight scaling relations. In order to obey the three local scaling relations by $z = 0$ – assuming no significant black hole growth – the distant spheroids have to grow their stellar mass by approximately 60% ($\Delta \log M_{sph} = 0.20 \pm 0.14$) in the next 4 billion years, while preserving their size and holding their stellar mass to light ratio approximately constant. The measured evolution can be expressed as $M_{BH}/M_{sph} \propto (1+z)^{1.5 \pm 1.0}$, consistent with black holes of a few 10^8 $M_\odot$ completing their growth before their host galaxies. Based on the disturbed morphologies of a fraction of the sample (6/20) we suggest collisional mergers with disk-dominated systems as the physical mechanism driving the evolution.

Subject headings: black hole physics: accretion — galaxies: active — galaxies: evolution — quasars: general

1. INTRODUCTION

In the local Universe, most galactic nuclei harbor a supermassive black hole (e.g., Kormendy & Richstone 1995). The mass of the black hole correlates with global properties of the host, such as the velocity dispersion and luminosity of the spheroidal (or bulge) component, indicating a connection between nuclear activity and galaxy formation and evolution (Magorrian et al. 1998; Ferrarese & Merritt 2000; Gebhardt et al. 2000, 2001; Marconi & Hunt 2003; Häring & Rix 2004; Novak et al. 2006; Graham & Driver 2007). Understanding the origin of this relation is a major challenge for cosmological models and is believed to hold the key to solving several astrophysical problems such as the role of feedback from nuclear activity in suppressing star formation in massive galaxies (e.g., Granato et al. 2004; Di Matteo et al. 2005; Croton et al. 2006; Malbon et al. 2006; Ciotti & Ostriker 2007).

In the standard cosmological scenario, spheroids grow by mergers of smaller galaxies while black holes grow by accreting surrounding matter. Depending on the relative timing of the two processes, the scaling relations between black hole mass and spheroid luminosity and velocity dispersion (hereafter M_{BH}-L – or M_{BH}-L_B to specify the blue band – and M_{BH}-σ relations, respectively) could also evolve with cosmic time. For example – if the spheroid evolved passively due to aging of stellar evolutions, changing L but not σ, while the black hole grows by accretion – we would expect evolution in both the M-L and the M-σ relations, with the latter evolving more slowly than the former. By contrast, if black holes completed their growth first and the dominant mode of growth now is the transformation of stellar disks into spheroids, the two relations would evolve in the opposite sense (Croton 2006). The tightness of the local relationships has been interpreted as evidence for feedback that synchronizes the relative growth. In this context, the tight relationships would be naturally reproduced if galaxies and black holes moved up the M-σ relation during merging events, so that the correlation would appear not to evolve with redshift (Haehnelt & Kauffmann 2000).

Detailed theoretical predictions are extremely difficult due to the daunting range of scales – ranging from the Mpc scale halo to the pc scale dynamical sphere of influence of the black hole, to the μpc scale of the accretion disk – and physical processes involved– radiative transfer, heating and cooling, accretion, just to name a few. In spite of the challenge, numerous groups have been able to develop models that are increasingly more successful at reproducing a variety of observations (e.g. Granato et al. 2004; Miralda-Escudé & Kollmeier 2005; Hopkins et al. 2006b; Croton et al. 2006; Malbon et al.

[1] Department of Physics, University of California, Santa Barbara, CA 93106-9530; tt@physics.ucsb.edu, woo@physics.ucsb.edu
[2] Alfred P. Sloan Research Fellow
[3] Department of Physics and Astronomy, University of California at Los Angeles, CA 90095, malkan@astro.ucla.edu
[4] Kavli Institute for Particle Astrophysics and Cosmology, Stanford, CA, rdb3@stanford.edu

2006; De Lucia & Blaizot 2007; Ciotti & Ostriker 2007). However, to this date, the evolution of scaling laws remains very uncertain and sensitive to the schemes and approximations adopted to deal with the complex physics (compare for example the recent works by Hopkins et al. 2007 and Robertson et al. 2006).

Accurate empirical measurements are needed to discriminate between scenarios, and provide input on the relative importance of various physical phenomena as well as on the accuracy of approximations. With this goal in mind, a number of groups have started observational programs to trace the evolution of scaling laws over cosmic time (Shields et al. 2003; Treu et al. 2004; Walter et al. 2004; Adelberger & Steidel 2005; Woo et al. 2006; McLure et al. 2006; Peng et al. 2006a,b; Salviander et al. 2006). However, observers face two fundamental limitations. On the one hand, – since the sphere of influence of supermassive black holes is too small to be resolved at cosmological distances with present technology – black hole mass estimates can only be obtained for active galaxies. Typically, this involves broad line AGN and the dynamics of the broad line region, with consequent loss of information about the host galaxy which is swamped by nuclear light. On the other hand – at a deeper level – the evolution of the scaling laws, depends on the interplay of at least four physical processes: i) black hole accretion; ii) evolution of the stellar populations; iii) dynamical evolution of the spheroid, e.g. through mergers; iv) black hole feedback on star formation. For this reason, even when a scaling law can be measured as a function of redshift, the interpretation is often times ambiguous. For example, as discussed by Peng et al. (2006b), how much of the evolution of the M-L relation is due to evolution in the spheroid mass and how much is due to evolution of the stellar populations?

In this paper we address the two fundamental limitations by adopting the following strategy. First, as in our pilot study (Treu et al. 2004) and in the first paper of this series (Woo et al. 2006, hereafter paper I), we focus on relatively moderate redshift ($z \sim 0.36$) and luminosity (monochromatic luminosity at 5100Å $\sim 10^{44}$ erg s^{-1}) AGN. Although the lookback time is considerably smaller than that of the most distant quasars studied by other groups, this choice allows us to determine the host galaxy properties with considerably smaller uncertainties. Second, we concentrate on a relatively small sample and measure several independent properties of the host galaxies. Paper I reported stellar velocity dispersion measurements based on Keck spectroscopy. This paper presents host spheroid luminosity and size measurements based on HST-ACS imaging. We use this combined dataset to study at the same time and for the same sample the M_{BH}-L and M-σ relations and the Fundamental Plane of host spheroids. The combination of these diagnostics – which can be thought as projections of a more fundamental manifold (e.g., Hopkins et al. 2007) – allows us to disentangle stellar mass growth, stellar population evolution and black hole growth, and helps to identify the processes at work (see also Ciotti & van Albada 2001; Nipoti et al. 2003; Boylan-Kolchin et al. 2006).

The paper is organized as follows. In § 2, we summarize the properties of the sample, describe the HST-ACS observations, and present our surface photometry. We also derive black hole masses using nuclear luminosities as measured from HST images and the new calibration of the broad line region size - nuclear luminosity relation (Bentz et al. 2006b), together with Hβ line widths from paper I. To construct a suitable local comparison sample, we use Sloan Digital Sky Survey images to derive new measurements of the spheroid luminosity of a sample of local Seyferts with M_{BH} available from reverberation mapping (Peterson et al. 2004; Bentz et al. 2006a). § 3 describes our main results, i.e. the Fundamental Plane, M_{BH}-L_B, and M_{BH}-σ relation of the distant Seyferts. Detailed estimates of systematic errors and selection effects are given in § 4. § 5 analyzes the three scaling relations under the assumption that the distant Seyferts will evolve to match the local relations and derives constraints on the evolution of stellar mass, size and stellar populations of the host spheroids as a function of black hole growth. The results are discussed and compared with the literature in § 6, and summarized in § 7.

Throughout this paper magnitudes are given in the AB scale. We assume a concordance cosmology with matter and dark energy density $\Omega_m = 0.3$, $\Omega_\Lambda = 0.7$, and Hubble constant H_0=70 kms^{-1}Mpc^{-1}.

2. DATA

2.1. *Sample selection and observations*

The sample discussed in this paper coincides with that discussed in paper I of this series, with minor exceptions. Two of the objects (S16 and S31) studied in this paper do not have Keck spectroscopy due to the unfavorable weather conditions at Keck when follow-up observations were planned. One of the objects with deep Keck spectroscopy (S28) has no ACS images because it was observed after the schedule of the Hubble program had been completed. As in our previous paper, except for S99 that was selected before SDSS data release 1 (DR1) (Treu et al. 2004), the objects were selected from the SDSS archive, based on the following criteria: i) spatially resolved in the SDSS images; ii) redshift between 0.35 and 0.37; iii) Hβ equivalent width and Gaussian width greater than 5 Å in the rest frame. Most of the objects were selected from DR-1, and the remaining ones (S21,S23, S26, S27) were selected from DR-2. After the initial selection based on these criteria, the SDSS spectra of the objects observable from Keck were visually inspected by two of us (TT and MAM) to check line identification. Objects showing strong Fe II nuclear emission (the main obstacle to velocity dispersion measurement) were eliminated from the sample. For example, for the run of September 2003, out of 33 observable objects, 8 were rejected on the basis of visual inspection (the mean and rms r' magnitude of the selected and rejected samples are consistent, 18.76 and 0.42 vs. 18.98 and 0.63, respectively). Of the remaining 25 objects, 12 were observed during the run, based on observability. The fraction of rejected is similar for following runs, although the total number of objects increases significantly in subsequent data releases. No color selection was imposed, although a post-facto analysis shows that the SDSS colors of the sample are intermediate between those of a quasar and those of an old stellar population, consistent with the comparable fraction of nuclear and stellar light inferred from the HST images in the rest of this paper.

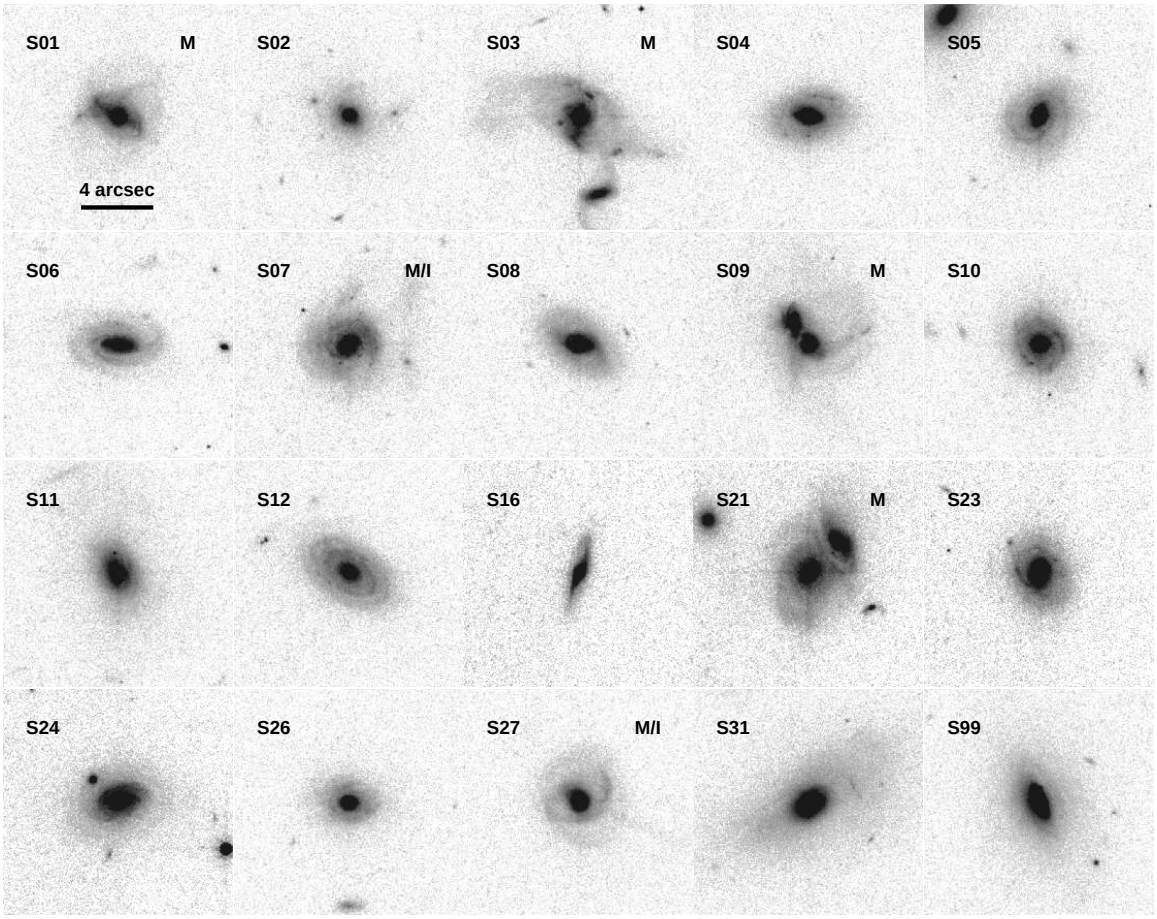

FIG. 1.— Postage stamp images of the 20 Seyfert galaxies in the sample. Each postage stamp is 12 arcseconds on a side, i.e. approximately 60kpc. Merging (Interacting) objects are identified by the label M (I). The centers of galaxies S11, S31 and S99 are obscured by dust lanes, which prevented accurate surface photometry of the nucleus and spheroid.

Coordinates, redshifts and other basic properties of the sample are given in Table 1.

The sample was observed using the Wide Field Camera of the ACS on board HST between August and December of 2004 as part of General Observer program 10216 (PI: Treu). Each object was observed for one orbit, split in four exposures dithered by semi-integer pixel shifts to ensure cosmic ray and defect removal as well as to improve sampling of the point spread function (PSF). The total exposure times range between 2148s and 2360s. Filter F775W (i') was chosen so as to sample the region corresponding to the rest frame 5100 Å in order to estimate the size of the broad line region, and to avoid contamination from the broad emission lines Hβ and Hα. This filter choice also provides spheroid luminosity redward of the 4000 Å break, and it is thus appropriate to infer spheroid structural parameters and rest frame B and V luminosity with minimal uncertainty due to filter transformations. Postage stamp images of the targets are shown in Figure 1.

2.2. *Reduction and analysis*

The following observables are needed to investigate our science questions: i) spheroid luminosity; ii) nuclear luminosity, to estimate the size of broad line region, and hence the black hole mass; iii) effective radius and effective surface brightness of the spheroid, to construct the Fundamental Plane. This section presents the measurements with an extensive discussion of systematic and random uncertainties.

2.2.1. *Reduction*

The images were reduced using MULTIDRIZZLE to remove cosmic rays and defects, correct for distortion and improve sampling of the PSF. Based on Monte Carlo simulations we adopted a final pixel size of 0.″04, which provides the best compromise between sampling of the PSF, signal to noise ratio of the individual pixels, and noise correlation.

2.2.2. *Surface photometry*

Surface photometry was derived using the GALFIT software (Peng et al. 2002) to fit two-dimensional models to the data. Optimizing a large number of non-linear parameters is a notoriously difficult problem, so we proceeded in steps, adding one component at a time. First, we fitted a point source to determine the center of the system, which is assumed common to all components. We then added a spheroid modeled as a de Vaucouleurs (1948) $r^{1/4}$ profile, and/or an exponential disk, if required by the χ^2 statistic. If needed, an additional component described by a Sersic (1968) profile with index n=0.5 was added to model the bar, identified as an elongated feature with a change in position angle with respect

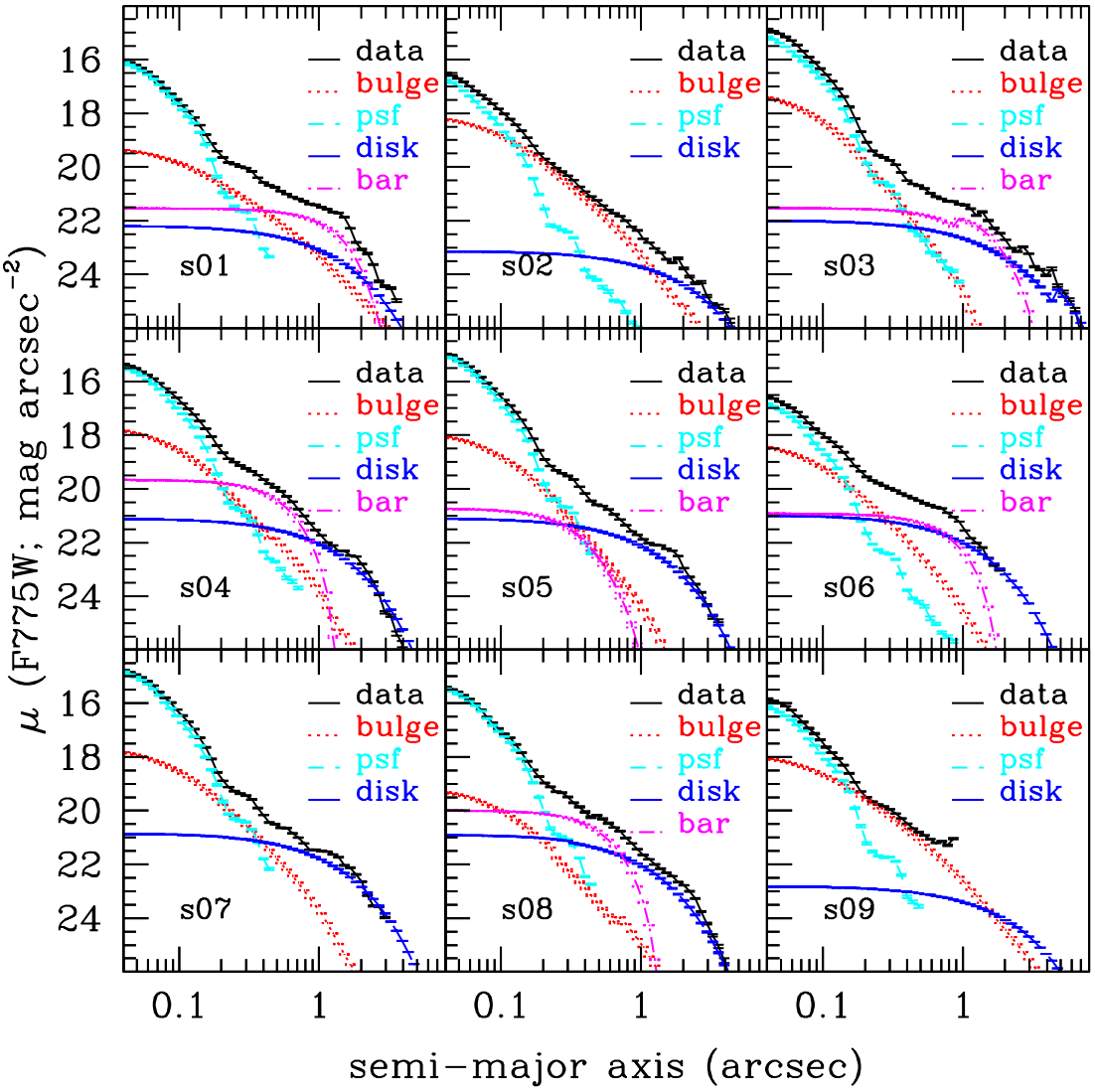

FIG. 2.— Surface photometry I. The surface brightness profile measured from the data are shown together with that determined from the two-dimensional model that best fits the data. The surface brightness profile of each component is shown separately to illustrate the relative contribution as a function of radius. Note that this plot is for illustration only, and the fits were performed in twodimensions as described in Section 2.2.2 using cutouts of 20″ on a side. The early truncation of a few profiles (e.g. S09) is only an artifact of the elliptical isophotes routine used to make the plots, due to nearby objects. For the measurement, the nearby objects were modeled and fitted simultaneously in twodimensions.

to the overall surface brightness distribution (see, e.g., S01 in Figure 1). Bars were found to be present in 7/20 cases and contribute between 4% and 16% of the total light. Extensive tests were conducted to ensure that the solution corresponded to the true global minimum of the χ^2 over the parameter space. Bright unsaturated stars in the field of the images were use to create a library of 43 point spread functions. Each galaxy was fitted with all the PSFs in the library to find the best fitting one as well as the best fitting parameters.

In three cases (S11, S31, S99), a prominent dust lane prevented us from determining accurate surface photometry. In two cases (S03 and S10) no stable solution with a sizable spheroid could be found, as the spheroidal component tended to become vanishingly small in size. Therefore we fixed the spheroid half light radius to 2.5 pixels (0.1 arcsec), the minimum size that could be resolved given our PSF and we considered the measured luminosity as an upper limit. Similarly, for three objects (S12, S21, S23) the measured spheroid half light radius is very close to our resolution limit (i.e. <3pixels), and therefore we also consider their luminosity as an upper limits. Extensive testing shows that the upper limit to the spheroid luminosity is robust with respect to the choice of the fixed half light radius, and of the PSF. Twelve out of twenty cases provided stable best fitting models and hence robust measurements. For illustration purposes one-dimensional surface brightness profiles (obtained with IRAF task ELLIPSE) are shown in Figures 2 and 3.

The formal statistical uncertainties on the spheroid luminosity are typically 0.05 mags. The rms scatter of the parameters for all the statistically acceptable PSFs was adopted as the systematic uncertainty due to PSF

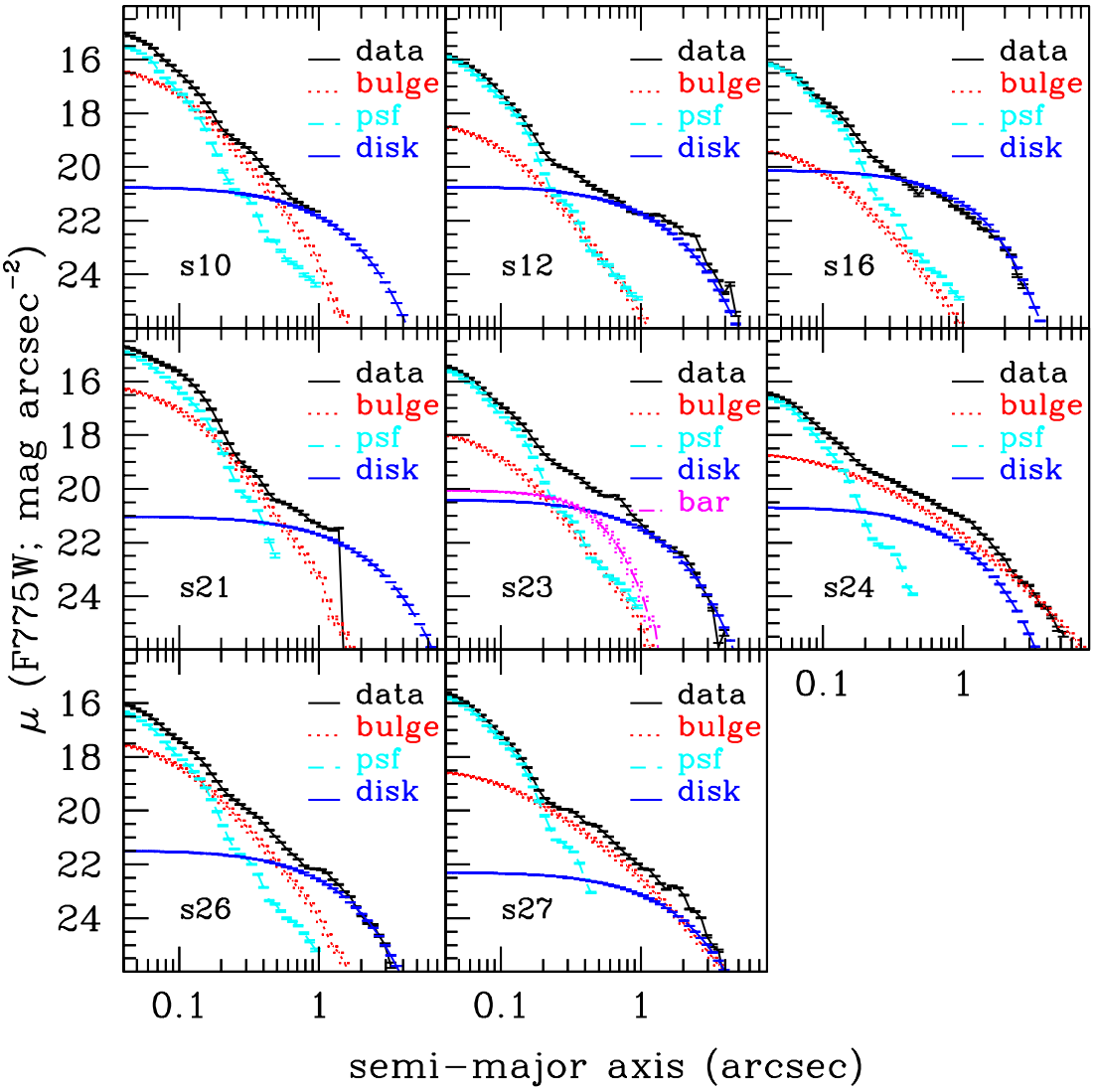

FIG. 3.— Surface photometry II. As in Figure 2 for the rest of the sample.

modeling. We estimated the total uncertainty – including systematic errors – by varying systematically all the fitting parameters and PSF, finding that the results are typically stable within 0.2 mags. Spheroid luminosity was then transformed into rest frame B-band luminosity by correcting for Galactic extinction and applying K-color corrections, calculated as described in Treu et al. (2001b). Errors on extinction and K-color corrections are a few hundredths of a magnitude. Conservatively, we adopt 0.5 mags (i.e. 0.2 dex) as the total uncertainty on spheroid luminosity. This uncertainty is smaller than the estimated uncertainty on black hole mass from single epoch measurements ∼0.4 dex and therefore sufficient to meet our goal of constructing the M-L_B relationship. Observed and intrinsic spheroid luminosities are given in Table 2.

Another source of systematic uncertainty is the choice of the surface brightness profile used to describe the spheroid. Although $r^{1/4}$ profiles are the traditional and widely used choice in the analysis of AGN host galaxies (e.g. Bentz et al. 2006a), detailed studies of nearby bulges show that Sersic profiles with lower Sersic index (typically 2-3) can provide a better fit. To estimate systematic errors on the spheroid luminosity associated with our choice of profile, we repeated our analysis using a Sersic profile with index 2 and 3 (Figure 4). As expected, we find that the best fit spheroid luminosity decreases with the Sersic index. Quantitatively, the spheroid luminosity decreases on average by 0.15 (0.33) mags when changing the Sersic index from 4 to 3 (2). Similarly, the point source luminosity increases on average by 0.02 (0.05) magnitudes and the effective radius of the spheroids decreases by 9% (11%) when changing the Sersic index from 4 to 3 (2). We thus conclude that adopting a $r^{1/4}$ profile provides a conservative measurement of the maximum luminosity of the spheroid and of the minimum nuclear luminosity (and hence M_{BH}). We will come back to this point in the discussion of our results in Section 4.2.

Other measurements of interest are total magnitude, nuclear luminosity at rest frame 5100Å (L_{5100}), the

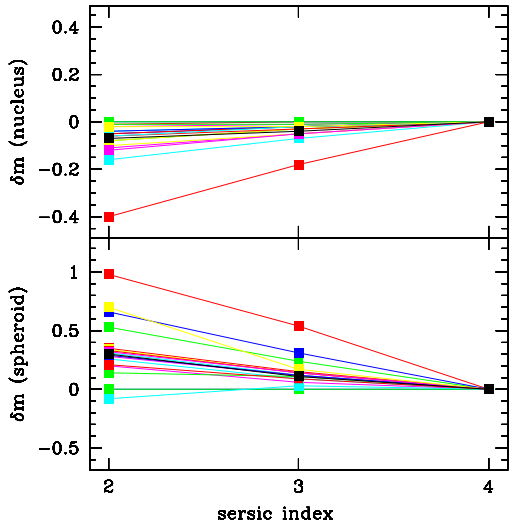

FIG. 4.— Systematic effects due to adopted spheroid profile. Changing the Sersic index of the spheroid from n=4 to n=3 (2), reduces systematically the spheroid luminosity by 0.15 (0.33) magnitudes, and increases the nuclear luminosity by 0.02 (0.05) magnitudes.

combination of effective radius (R_e) and effective surface brightness (SB_e) that enters the Fundamental Plane $FP_{ph} = \log R_e$ - 0.32 SB_e (see 3.1) and the fraction of nuclear light (f_{nuc}). The total uncertainties, conservatively estimated as for the spheroid luminosity, are 20% on L_{5100} and on f_{nuc}, and 0.1 on FP_{ph}. The relevant quantities are also listed in Table 2.

2.3. *Black hole mass*

As in paper I of this series, black hole masses were derived from the width of Hβ and the observed nuclear luminosity at 5100 Å, using the so-called 'virial' method or empirically calibrated photoionization method (Wandel et al. 1999; Vestergaard 2002; Vestergaard & Peterson 2006). Briefly summarized, the method assumes that the kinematics of the broad line region trace the gravitational field of the central black hole. The width of the line provides the velocity scale, while the nuclear continuum luminosity provides the size via the empirical correlation observed for the local reverberation mapped sample (Wandel et al. 1999; Kaspi et al. 2000, 2005; Bentz et al. 2006b). The virial coefficient is obtained by requiring that local AGN hosts and quiescent galaxies obey the same M-σ relation (Onken et al. 2004; Greene & Ho 2006). This method has been shown to provide an estimate of the black hole mass within a factor of 2-3. For this paper we will assume as in the previous paper of the series a nominal uncertainty of 0.4 dex on black hole mass obtained with this method (see Peterson 2007, for a recent discussion of the method). However, since we allow for unknown intrinsic scatter in the scaling relations when fitting for the intercept (§ 3), adopting a larger random uncertainty on each individual black hole mass estimate (e.g. 0.6 dex, Vestergaard & Peterson 2006) has a negligible impact in terms of overall uncertainty (§ 4.3).

As in paper I, we adopt the second moment of the broad component of Hβ as our velocity scale since this is more robustly measured than the alternative FWHM (paper I; see also Peterson et al. 2004; Collin et al. 2006). The velocity scale is measured from Keck spectra when available and from SDSS spectra in the few cases when Keck spectra are not available (see paper I for details). As shown in paper I, our methodology gives unbiased black hole masses when applied to the local sample of calibrators. A major improvement with respect to paper I is that we can use high resolution Hubble images to measure the nuclear luminosity and infer broad line region size. In practice we use the following equation to estimate black hole masses, obtained combining the most recent calibrations of the size luminosity relation and virial coefficients (Onken et al. 2004; Bentz et al. 2006a).

$$\log M_{\rm BH} = 8.58 + 2\log\left(\frac{\sigma_{\rm H\beta}}{3000{\rm kms}^{-1}}\right) + 0.518\log\left(\frac{L_{5100}}{10^{44}{\rm ergs}^{-1}}\right), \quad (1)$$

where $\sigma_{H\beta}$ is the second moment of the broad Hβ line profile. We note that for the sample in common with paper I, the use of nuclear luminosities and this new calibration implies black hole masses smaller by 0.09 dex on average, consistent with our estimate of the magnitude of this systematic error in paper I. Black hole masses are listed in Table 2.

2.4. *Local comparison samples*

To study evolutionary effects we consider two comparison samples to define the local M-L_B relation. First we consider the sample of quiescent galaxies collected by Marconi & Hunt (2003). The sample consists of galaxies with black hole mass determined from spatially resolved kinematics and with spheroid luminosity determined from two-dimensional surface photometry. The second sample is that of local Seyfert galaxies with black hole mass measured via reverberation mapping discussed in Peterson et al. (2004) and Onken et al. (2004). To ensure self-consistent determination of spheroid luminosity for the local and distant Seyfert sample we measured the parameters of the local sample in exactly the same way as we do for distant galaxies. We searched the SDSS archive for g'-band images of local Seyferts, which provide a very good match to our distant galaxies in terms of resolution (the seeing is typically 10 times the HST PSF, but the angular size distance is typically 10 times smaller) and rest frame wavelength. SDSS images for nine Seyferts were found in the archive. The resulting spheroid luminosities for the local Seyfert samples are listed in Table 3, together with redshifts, black hole masses and velocity dispersions from the literature.

The two samples are complementary in terms of vices and virtues. The first sample is larger in size and black hole masses, and spheroid luminosities are most robustly measured: i) M_{BH} is obtained from spatially resolved kinematics; ii) the determination of spheroid luminosity does not suffer from poor resolution or the presence of a prominent point source in the center. However, the second sample is the most appropriate for a direct comparison for a variety of reasons: i) the virial coefficient is unknown, but assuming that it is not evolving with redshift, the comparison between Seyfert samples is independent of its numerical value; ii) if the local M-L relation is not universal, Seyferts may define a different M-L relation than quiescent early-type galaxies – perhaps because they are at a different evolutionary stage. Thus,

we conclude that at this stage the more conservative approach is to consider both samples for the following analysis and consider the uncertainty on the local relation as an additional source of systematic errors. More comprehensive studies of the local M-L relation are needed to eliminate this source of uncertainty. This is left for future work.

3. RESULTS

This section presents the main results of this paper. First in § 3.1 we discuss the Fundamental Plane of the host galaxies in comparison with that of normal quiescent galaxies, for the subsample of objects that have both σ and structural parameters. In § 3.2 we present the M_{BH}-L_B relation for distant Seyfert galaxies. Having established that the Fundamental Plane of the host galaxies is indistinguishable from that of quiescent galaxies, we adopt the luminosity evolution inferred from FP analysis (Treu et al. 2005a,b) to compare with the local M_{BH}-L_B relation. In § 3.3 we revisit the M_{BH}-σ relation derived in paper I, using the new improved black hole mass estimates based on nuclear luminosities determined from HST imaging.

3.1. *Fundamental Plane*

In the local Universe early-type galaxies obey the Fundamental Plane, i.e. an empirical correlation between effective radius, central velocity dispersion and effective surface brightness of the form:

$$\log R_e = \alpha \log \sigma + \beta \mathrm{SB_e} + \gamma, \qquad (2)$$

with $\alpha = 1.25$, $\beta = 0.32$ and $\gamma = -9.00$ for the Coma Cluster in the B(AB) band. The evolution of the FP out to redshift $z \sim 0.4$ is well established for quiescent early-type galaxies (e.g., Treu et al. 2005b, 2001a, and references therein), for AGN hosts (Woo et al. 2004, 2005), and for the spheroidal component of spiral galaxies with bulge-to-total luminosity ratio greater than 0.2 (MacArthur et al. 2007, in preparation).

In Figure 5 we plot the FP parameters of the subset of distant Seyferts for which structural parameters and stellar velocity dispersion is available, together with a comparable sample of quiescent galaxies taken from Treu et al. (2005a,b). The good agreement between the FP of quiescent and active galaxies gives us confidence that our surface photometry is not systematically biased by the presence of a nuclear point source. The offset with respect to the local relation (solid line) is normally interpreted as evolution of the stellar populations. Under the assumption of pure luminosity evolution, luminosity evolves with redshift such that the expected value at $z = 0$ is given by

$$\log L_{B,0} = \log L_B - (0.72 \pm 0.06 \pm 0.04) z \qquad (3)$$

(Treu et al. 2005b). Applying the same assumption to the sample of distant Seyferts at $z = 0.36$ implies that: $\log L_{B,0} = \log L_B - 0.26 \pm 0.03$, where random and systematic errors have been added in quadrature for simplicity.

3.2. *M_{BH}-L_B Relation*

In order to compare with the local relations we need to account for the fact that the luminosity of a stellar population decreases as it ages. As our first working hypothesis, in this Section we will present our results assuming that stellar populations evolved as inferred from the FP studies under a pure evolution scenario, and use the variable $L_{B,0}$ obtained using equation 3. A more general discussion will be given in § 5.

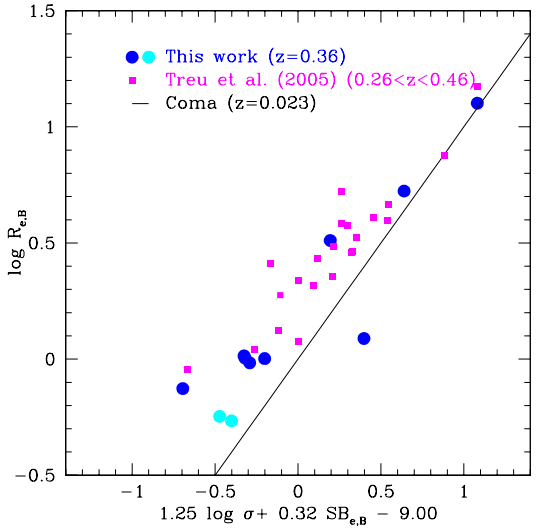

FIG. 5.— Edge on view of the Fundamental Plane of the distant Seyfert galaxies (circles) and of normal quiescent galaxies at comparable redshift (squares). Seyfert galaxies for which only an upper limit to the spheroid luminosity is available are plotted as cyan symbols. The errors on the FP variables are highly correlated, and points are allowed to move mostly within the plane. The error component perpendicular to the plane is estimated to be ~ 0.1 dex for the Seyfert sample when projected along the $\log R_e$ axis. Most of the apparent thickness of the FP for quiescent galaxies is due to the relatively large range in redshifts and luminosity evolution during the corresponding interval in cosmic time. The local FP of the Coma Cluster is shown as a solid black line for comparison.

The relation between black hole mass and host spheroid luminosity for our points as well as for local comparison samples is shown in Figure 6. The main result is that the Seyfert galaxies at $z = 0.36$ and those at $z = 0$ cover approximately the same range in spheroid luminosity, but the average black hole mass is higher for the distant Seyferts. The mismatch is exacerbated if one considers that five of the distant Seyferts measurements are upper limits (while only one of the local Seyferts is an upper limit). Conservatively we will generally consider the measured offset as the best estimate of the offset although it should be kept in mind that it is most likely a lower limit. Quantitatively, the offset with respect to the fiducial local relationship (solid line) corresponds to $\Delta L_{B,0} = 0.32 \pm 0.11 \pm 0.15$ ($\Delta \log M_{BH} = 0.40 \pm 0.14 \pm 0.19$), considering the intrinsic scatter of the relation to be a free parameter and then marginalizing over it. Listed systematic errors are derived as discussed in Section 4. If measured with respect to the local Seyferts (magenta line), the best estimate of the offset changes to $\Delta \log M_{BH} = 0.63$. This is visualized in Figure 7 where we plot the distribution of residuals with respect to the local fiducial relation for the distant and local samples.

We conclude that pure luminosity evolution is inconsistent with the observations, if we required that at $z = 0$ all galaxies obey the M_{BH}-L_B relation. We cannot solve this

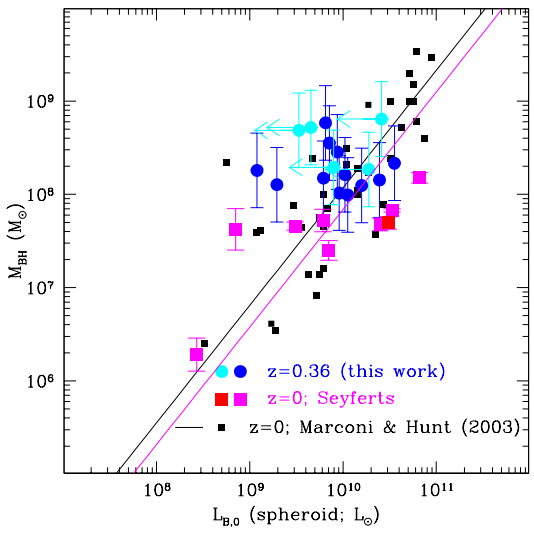

FIG. 6.— Black hole mass spheroid luminosity relation. Distant Seyferts are shown as large circles with error bars. Blue circles represent measurements, cyan circles with leftward arrows represent upper limits to the spheroid luminosity. Local Seyferts are shown as large squares with error bars. Black hole masses are from Peterson et al. (2004) and Bentz et al. (2006b), spheroid luminosities are from this work (Table 3). Magenta squares represent measurements, the red square represents an upper limit to the spheroid luminosity. Small black squares represent local quiescent galaxies from (Marconi & Hunt 2003). The black line is the best fits to the Marconi & Hunt (2003) sample. The magenta line is the best fit to the local Seyferts. For direct comparison the spheroid luminosity of the distant Seyferts has been evolved to $z = 0$ using $\log L_{B,0} = \log L_B - 0.26$ (see § 3.2).

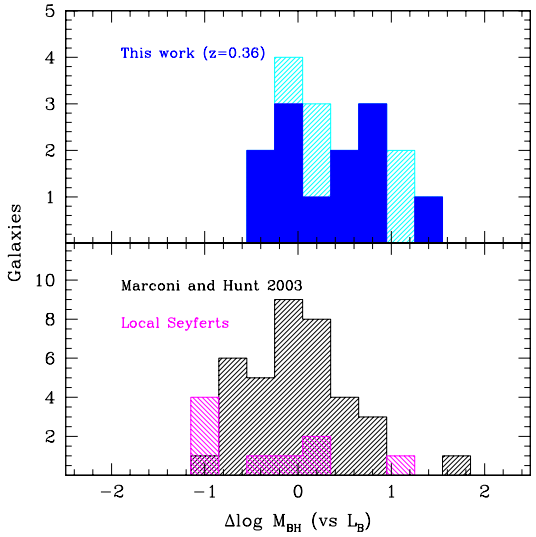

FIG. 7.— Distribution of residuals in $\log M_{BH}$ with respect to the fiducial local relation of Marconi & Hunt (2003, solid black line in Figure 6). The Upper panel shows distant Seyferts (measurements in blue, upper limits in cyan; note that upper limits in $\log L_{B,0}$ correspond to lower limits in $\Delta \log M_{BH}$). The lower panel shows the distribution of residuals for the local samples of quiescent and Seyfert galaxies.

inconsistency by invoking different luminosity evolution. The stellar populations would be required to become brighter with time in order to reconcile the data with the local relationship. This can be ruled out on physical grounds. Therefore, taking this result at face value, we have to conclude that either not all spheroids obey the M-L relations, or that a significant amount of new stars have been added to the spheroids since $z = 0.36$. The interpretation of this result will be discussed in Sections 5 and 6, after we conclude presenting the evidence and discussing systematic errors and selection effects in the remainder of this section.

3.3. M_{BH}-σ Relation

Figure 8 shows the M_{BH}-σ relation for the distant Seyferts as well as the local comparison samples. The samples and symbols are the same as in Figure 6 with few minor exceptions: i) only the 14 distant Seyferts with available stellar velocity dispersion (from paper I) are plotted, including S28 and S99 for which HST photometry is not available. ii) local relations are from Tremaine et al. (2002) and Ferrarese & Ford (2005); iii) Local Seyferts obey the same relation as quiescent galaxies by construction, as this is the constraint used to derive the virial coefficient (Onken et al. 2004), so there is no need to show a separate local relation for Seyferts. The only substantial difference with respect to Figure 8 in paper I is that black hole masses have been recalculated based on HST photometry.

The M_{BH}-σ relation shows the same basic result as the M_{BH}-L_B relation. At fixed host galaxy properties,

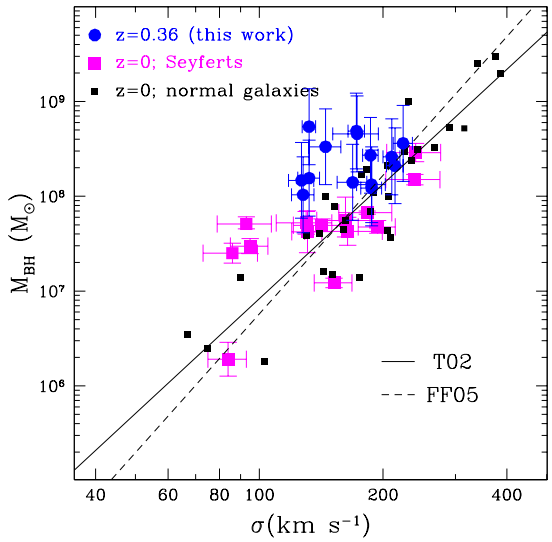

FIG. 8.— Black hole mass velocity dispersion relation. The large blue circles represent distant Seyferts. Black hole masses are from this work, velocity dispersions are from paper I. The large magenta squares represent local Seyferts, the small black squares represent local quiescent galaxies. The solid and dashed lines are the best fit relations from Tremaine et al. (2002) and Ferrarese & Ford (2005). The local Seyferts obey the same M_{BH}-σ relation as local quiescent galaxies by construction, see Onken et al. (2004) for discussion.

distant Seyferts appear to host larger black hole mass than local ones. Quantitatively, the offset corresponds to $\Delta \log \sigma = 0.13 \pm 0.03 \pm 0.05$ (i.e. $\Delta \log M_{BH} = 0.54 \pm 0.12 \pm 0.21$). Note that offset is slightly reduced (0.08 in $\Delta \log M_{BH}$) with respect to paper I and the systematic error is smaller due to the improved estimate of black hole masses that avoid stellar contamination. As shown in Figure 8 and discussed in paper I, adopting the local relation from Tremaine et al. (2002)

or Ferrarese & Ford (2005) changes the offset by much less than the error bars because the two local relations are very well matched in the range of black hole mass and stellar velocity dispersion covered by our sample.

4. SYSTEMATICS AND SELECTION EFFECTS

This section is devoted to understanding and estimating systematic errors. First, in § 4.1 and § 4.2, we list potential sources of systematic error and estimate as accurately as possible the associated uncertainty. For brevity we will not repeat the analysis of systematics already discussed in paper I, unless when substantial changes/improvements are introduced. § 4.3 derives the uncertainty on our estimate of the random errors due to our assumed accuracy of single-epoch black hole mass determinations. Then, in § 4.4, we introduce a Monte Carlo scheme to simulate unknown selection effects and estimate potential biases. § 4.5 gives a very short summary of this Section for the impatient reader.

4.1. *Is M_{BH} overestimated?*

Understanding the M_{BH} estimate is clearly important. While velocity dispersion and spheroid photometry are measured independently and present mutually consistent results (as supported by the FP relation, which does not involve M_{BH}), only one measurement of M_{BH} is available and that determines the evolution of both relationships. Our measurement of M_{BH} depends on two observables (velocity scale and nuclear luminosity), on the empirically calibrated relationship between nuclear luminosity and broad line region size and on the choice of the virial coefficient. We now go through each source of error and estimate the systematic error that they may introduce for a sample of our size.

4.1.1. *Hβ line width and velocity scale*

In paper I we demonstrated that our measurement of the velocity scale from the second moment of Hβ in single epoch spectra is unbiased. This means that – when applied to the sample of local calibrators – our estimator yields the same M_{BH} as obtained by the original studies based on the second moment of Hβ measured from the variable part of the spectra. Recently, Peterson (2007) suggested that single epoch spectra may overestimate the line width by ∼20%, corresponding to an error of ∼0.15 dex on black hole mass, if the same virial coefficient is assumed. This effect is likely to depend on the setup of the experiment and on the variability pattern. However, to be conservative, we will consider this as a global uncertainty to the zero point of our measured black hole mass. Woo et al. (2007) studied the time variability of the width of Hβ for a subset of our objects. They found that the r.m.s. variations of the second moment of Hβ are less than 14% (i.e. $\sim$ 0.1 dex in M_{BH}). For our sample of 14-17 objects this has therefore negligible effect on the average with respect to the aforementioned source of error. Our best estimate of overall systematic uncertainty due to line width measurement is 0.15 dex.

To check for systematic effects due to systematic change of the line shape with redshift or sample properties such as Eddington Ratio (e.g., Collin et al. 2006) we also computed black hole masses using the full width half maximum instead of the second moment of the line as velocity scale. After removing the narrow component of Hβ using [O III] as a template as described in Treu et al. (2004) and Woo et al. (2006), we measured the FWHM (McGill et al. 2007, in preparation) and derived black hole mass estimates Using Eq. 1 in Netzer & Trakhtenbrot (2007). This alternative estimate of black hole mass ($M_{BH,NT}$) agrees very well with that adopted in this paper, with an average offset of $\langle \log M_{BH}/M_{BH,NT} \rangle = -0.02 \pm 0.05$ dex, i.e. consistent with no offset.

4.1.2. *Nuclear luminosity and size luminosity relation*

The new calibration of the size-luminosity relation (Bentz et al. 2006a), and our HST based nuclear luminosities are a substantial improvement with respect to paper I, allowing us to avoid issues related to host galaxy contamination. The dominant source of error is now the intrinsic scatter of the size luminosity relation (30%) corresponding to $\sim$ 0.1 dex in M_{BH} per individual object. For our sample size, this translates into a negligible source of error in the mean. As far as the overall calibration of the relation is concerned, for the luminosity range of our sample, the 68% range on the slope and intercept of the relationship translate into an overall uncertainty in size of order 0.02 dex. We thus conclude that the uncertainty due to the (known) scatter of the size luminosity relation is negligible.

4.1.3. *Virial coefficient and zero point of the local relation*

The final source of error is related to the virial coefficient needed to convert size and velocity scales into mass and thus to the zero point of the local relation. As discussed in detail in paper I, we adopt the virial coefficient determined by Onken et al. (2004) requiring that the M-σ relation be the same for local quiescent and active galaxies. The uncertainty on the average of the virial coefficient is 34%, thus corresponding to an uncertainty of 0.13 dex on the calibration of the black hole mass. However – as discussed in paper I – assuming that the virial coefficient does not evolve with redshift, this factor cancels out between the local and distant samples and therefore is irrelevant. Incidentally, we note that our results can also be interpreted as cosmic evolution of the virial coefficient, if one is willing to drop this assumption. We consider this an unlikely explanation, as it would require the geometry or kinematics of AGN to evolve with cosmic time, but unfortunately it will not be possible to discard it until direct measurements of the virial coefficient can be obtained in some other way.

The situation is slightly more complex for the M_{BH}-L relation. Once the virial coefficient is fixed there is no more freedom. Therefore the difference between the intercept of the relation for local active and quiescent (0.23 dex in M_{BH}) is an additional source of uncertainty. Larger samples of galaxies with well determined black hole mass and spheroid luminosity are needed to overcome this limitation. For the purpose of this paper we consider the difference as an additional source of uncertainty. To produce a single measurement, we weight the two samples equally (for reasons discussed in § 3) and take the average and semi-difference of the two intercepts as best estimate of the local average and systematic uncertainty on the zero point ($\sim$ 0.12 dex).

4.2. *Is L_B underestimated?*

The main sources of uncertainty that could affect the spheroid luminosity of the sample as a whole are systematic errors in K-corrections, in the adopted luminosity evolution, and in the choice of the surface brightness profile for the bulge. The uncertainty on the K-correction is negligible, at most 0.02 dex, as estimated using a range of stellar population models to compute the transformation from observed F775W to rest frame B. The luminosity evolution as measured from the Fundamental Plane (Treu et al. 2005a) carries an overall uncertainty of 0.03 dex. Even assuming that this translates to a shift of the whole sample, this is still a negligible source of error. As discussed in Section 2.2.2 adopting a Sersic profile instead of a $r^{1/4}$ profile tends to systematically reduce the bulge luminosity while increasing the point source luminosity, and therefore black hole mass, thus moving points further away from the local M-L relation of quiescent galaxies. In contrast, since we used the same identical technique for the local Seyferts, adopting a Sersic profile would not alter the observed offset. We conclude that the measured offset is not overestimated by an appreciable amount due to known systematic errors on spheroid luminosity determination.

4.3. *Are random errors underestimated?*

Finally, the uncertainty of black hole mass estimates from single epoch data is assumed to be 0.4 dex (Vestergaard 2002). This represents all sources of random error that contribute to the scatter in Eq. 1. After quantifying sources of systematic errors on the mean of Eq 1, we now consider whether the random error associated with our measurement of the offset of the scaling relations could be underestimated. To test this, we repeat the analysis assuming that the random error on each individual M_{BH} estimate is 0.6 dex (Vestergaard & Peterson 2006). The inferred random error on $\Delta \log M_{BH}$ increases by 0.03 dex, e.g. from 0.14 dex to 0.17 dex for the M_{BH}-L relation. Note that our analysis includes a nuisance parameter to account for the unknown intrinsic scatter of scaling relations and therefore the estimated errors are slightly different than what would be naively derived considering only errors on the y axis ($0.4 / \sqrt{N-1} = 0.4/4 = 0.1$ dex vs $0.6/\sqrt{N-1}$=0.15). This is a negligible error on the error, considering that the systematic term is dominant. The total error, defined as the quadratic sum of the random and systematic uncertainties, would only change by 0.01 dex.

4.4. *Selection bias*

In this section we estimate possible bias due to selection effects. Our galaxies are selected based on their nuclear properties (having a broad line AGN). Therefore, intrinsic scatter and observational errors in the scaling relations could conceivably lead us to favor large black hole masses and therefore overestimate evolution[5].

Our present sample covers approximately a decade in black hole mass ($10^8 - 10^9 M_\odot$). The upper limit is naturally expected because of the steep drop of the black hole mass function. Is the lower limit in mass a result of some unknown selection effect? Our nominal selection limits on line width and flux are small enough that we would have been able to select objects with black hole masses as low as 10^7 $M_\odot$, as verified by running our measurement tools on the entire SDSS-DR5 spectroscopic database at this redshift. However the objects with M_{BH} well below $10^8 M_\odot$ are a small fraction of the total. This maybe be due to an intrinsic drop in the black hole mass function, to a selection effect in the SDSS spectroscopic sample or to a combination of the two. The decline in the number of objects at $z = 0.36$ with M_{BH} well below 10^8 is also seen in Figure 1 of Netzer & Trakhtenbrot (2007), where most of the points lie above the group identified as having M_{BH} between $10^{7.5}$ and $10^{7.8}$ $M_\odot$. Estimating the black hole mass function is beyond the scope of this work (e.g., Bernardi et al. 2006; Greene & Ho 2007). However, to understand the implications of this selection effect on our measurement, we can take a conservative approach and model this drop as a sharp selection in M_{BH}. In the following discussion we assume for reference that our implicit selection function $\log M_{BH}/M_\odot > 7.9$ (the results are unchanged if the limit is chosen to be 7.8 or 8.0). We then use Monte Carlo simulations to determine the amount of bias on the offset of the intercept of the scaling relations introduced by the implicit selection process. The scaling relations are populated according to the velocity dispersion function and spheroid luminosity function determined by Sheth et al. (2003) and Driver et al. (2007) respectively, and errors on both axis are taken into account. We assume that the intrinsic scatter of the relation is smaller than the measurement errors (0.4-0.5 dex) which is consistent with local estimates. Note that in this scheme all the selection procedure is modeled a single hard threshold in black hole mass and we only work in the scaling relation variables. This simple scheme allows us to bypass all the assumptions that would be needed to simulate from first principles the observational selection effects which are a complex combination of total flux, broad line flux, broad line width (at both ends), bulge luminosity and stellar velocity dispersion.

The results of the simulations are shown in Figure 9. The curves show the recovered ("measured") offset as a function of the input offset $\Delta \log M_{BH}$. The upper panel shows the results for the M_{BH}-σ relation, the lower panel shows the results for the M_{BH}-L relation. The bias is almost negligible for the M_{BH}-σ relation, while it is at most 0.1 dex for the M_{BH}-L relation. The difference between the two relations is due to: i) the smaller errors on velocity dispersion than those on spheroid luminosity; ii) the different behavior of the two distributions at the faint (low velocity) end. The velocity dispersion function peaks in the range covered by our sample, while the luminosity function of bulges extends to much smaller luminosities. As a softer cutoff would imply smaller bias, we conclude that selection effects are responsible for at most 0.1 dex of the observed offset of the M_{BH}-L relation, and that this source of bias is negligible for the M_{BH}-σ relation.

4.5. *Summary of uncertainties and best measurements*

In conclusion, the total systematic error on the evolution of M_{BH}-σ relation is 0.21 dex in M_{BH} (i.e. slightly reduced with respect to paper I due to the improved nuclear luminosity estimates), and 0.19 on the M_{BH}-L re-

[5] This bias is similar to Malmquist bias for luminosity selected samples of standard candles

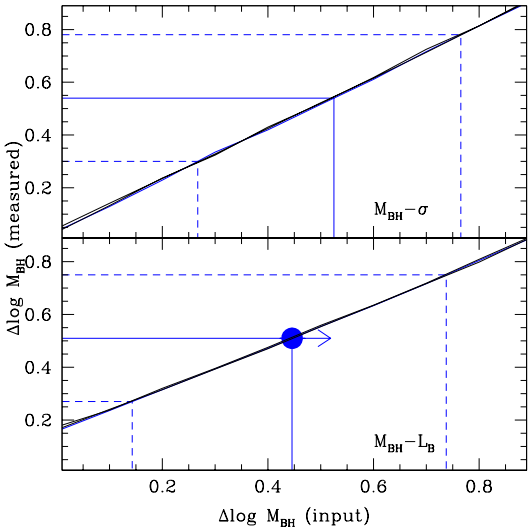

FIG. 9.— Estimate of possible bias due to selection effects. The effects on an hypothetical selection $\log(M_{BH}/M_\odot) > 7.9$ are calculated via Monte Carlo simulations (see § 4.4 for details). The measured offset is shown as a function of the simulated input offset in M_{BH} with respect to the local relation. **Upper panel: results for the M_{BH}-σ relation**. The bias is negligible due to the small error on σ (compared to that on M_{BH}) and the flatness of the velocity dispersion function in the range of interest. The measured offset and the corresponding input offset are identified by the solid blue lines. Dashed lines identify error bars obtained by summing in quadrature random and systematic errors. **Lower panel: results for the M_{BH}-L_B relation**. The bias is somewhat more significant due to the larger error on L_B and to the steeper faint end of the spheroid luminosity function. The solid blue line and large filled circle identify the lower limit to the offset as measured with respect to the average of local quiescent and active galaxies. Dashed lines represent error bars as in the upper panel.

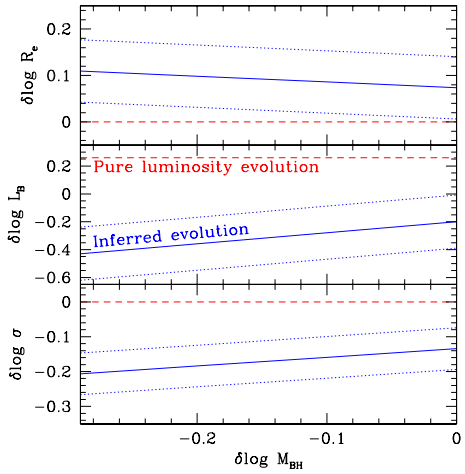

FIG. 10.— Inferred evolution of the fundamental manifold parameters (solid blue lines), as a function of change in black hole mass. Dotted blue lines represent the 68% confidence bands. The symbol δ indicates the difference between the parameter at $z = 0.36$ and the parameter at $z = 0$. The red dashed horizontal lines represent pure luminosity evolution of the host galaxies for reference. If there is no black hole growth ($\delta \log M_{BH}$=0) the host galaxies of the distant Seyferts need to increase their velocity dispersion by 0.13 ± 0.06 dex and increase their luminosity by 0.20 ± 0.19 dex in the next 4 Gyrs in order to obey simultaneously the local FP, M_{BH}-σ, and M_{BH}-L_B relations, with no significant change in the effective radius. For comparison, pure luminosity evolution of the spheroid would predict 0, -0.26 and 0, respectively (dashed red lines). This corresponds to a growth of ∼60% of the spheroid stellar mass and approximately constant stellar mass-to-light ratio. If there is significant black hole growth ($\delta \log M_{BH} < 0$) the increase in σ and L_B and the decrease in effective radius must be more pronounced.

lation, dominated by the uncertainty on the black hole mass and on the uncertainty on the local relation.

Although we caution the reader to keep in mind all the caveats discussed above, we now condense all the information discussed in this section in seven numbers. Our best estimates of the offset of the relations – without accounting for selection effects are:

- M_{BH}-L: $\Delta \log M_{BH} = 0.51 \pm 0.14 \pm 0.19$
- M_{BH}-σ: $\Delta \log M_{BH} = 0.54 \pm 0.12 \pm 0.21$

Unknown selection effects could remove as much as 0.1 dex to the offset of the M_{BH}-L relation.

5. EVOLUTION OF THE FUNDAMENTAL MANIFOLD OF BLACK HOLES AND SPHEROIDS

In the previous sections we concluded that pure luminosity evolution is inconsistent with the observations and the requirement that the distant Seyferts lie on the local relations. In this section, we explore the evolutionary constraints that can be obtained by examining the evolution of black holes and spheroids in a four dimensional parameter space – with axes given by luminosity, velocity dispersion, size and black hole mass – instead that on lower dimension spaces.

In other words, we know that in the local universe, black holes and their host spheroids lie on the FP, the M_{BH}-σ and M_{BH}-L relations – 3 relationships involving 4 parameters. Thus, by requiring that our distant galaxies land on the local relationships at $z = 0$, we can derive constraints on the evolution in size, luminosity and mass of the host galaxies, as a function of black hole growth in the same time span.

The results of this exercise are shown in Figure 10. For simplicity, systematic and random errors are combined in quadrature in order to compute confidence bands, and neglecting covariance. The main result is that in order to satisfy all scaling relations in the local universe the host galaxies have to grow in luminosity and velocity dispersion, while leaving the size substantially unchanged.

Consider the no black hole growth scenario (consistent with the low Eddington ratios, see paper I). Assuming that $M_{sph} \propto \sigma^2 R_e$, the spheroid mass has to increase by 0.20 ± 0.14 dex (∼ 60%), by today. In other words,

$$\frac{M_{BH}}{M_{sph}} \propto (1+z)^{1.5 \pm 1.0} \quad (4)$$

Similarly, the spheroid luminosity has to increase by 0.20 ± 0.19 dex, implying that its average stellar mass to light ratio has to stay approximately constant (with an uncertainty of approximately 50%) over the next 4 Gyrs. This requires an injection of younger stars to counteract the ageing of the resident population. The effective radius does not change significantly $\delta \log R_e = 0.07 \pm 0.07$. Those trends are amplified if significant black hole growth is assumed.

Although at this stage the measurement uncertainties do not allow firm conclusions, it is clear that this empirical methodology holds great promise as a way to

disentangle evolution of the stellar populations, black hole growth, and dynamical evolution of the host. In the future, with larger samples covering a wider range of masses and redshifts, it will be possible to study in the detail the co-evolution of spheroids and black holes, perhaps in the framework or more fundamental underlying correlations such as that proposed by Hopkins et al. (2007).

6. DISCUSSION AND CONCLUSIONS

In previous sections, we have presented evidence that just four billion years ago, there was a population of supermassive black holes living in smaller and less luminous spheroids than today. Based on a detailed analysis of uncertainties and selection effects, this evolutionary signature appears significant at the 95% CL. In this section we will briefly discuss our results in the broader context of galaxy formation and evolution and identify a possible physical mechanism. However, before discussing the interpretation of this result, it is worth mentioning two caveats (see also the discussion in paper I). i) Our measurement relies on M_{BH} estimates based on an empirically calibrated method. The sample of local calibrators is very small and does not necessarily match exactly the properties of our distant sample. More work on the local and distant samples remains to be done before unknown systematics can be firmly ruled out. ii) The local scaling relations are based on very limited samples. The quiescent sample consists of approximately 40 objects. In addition to the intrinsic difficulty of resolving the sphere of influence, the local sample is composed of earlier type galaxies than the sample considered here. As discussed in paper I, the two samples may have an evolutionary sequence built in at the selection. In this respect, the local AGN sample is very important, as the selection process and properties are very similar to those of our own sample. However the local AGN sample is comparable or smaller in size to our distant sample, and therefore it is hard to identify subtle differences which could point to some unknown selection effect.

Keeping these two caveats in the back of our minds, we move on to discuss and interpret the main result of this paper, that black hole mass growth appears to be completed before bulge growth. An important clue is given by the morphology of the host galaxies, provided by the HST images. The majority of galaxies in our sample are not spheroid-dominated elliptical or lenticulars, but rather intermediate or late type spirals. Most remarkably, as shown in Figure, 6/20 galaxies are observed to show signs of a major ongoing merging (3) or to be morphologically disturbed (3). Considering only the three most extreme cases and assuming that major mergers are visually identifiable for ∼0.5-1 Gyr (Cox et al. 2006b,a), this finding implies that most or possibly all the galaxies in our sample will undergo a major merger in between the time of observation and today. Gas-rich mergers are believed to be the main mechanism transforming stellar and gaseous disks into stellar spheroids, leading to substantial increase in spheroid luminosity and velocity dispersion. By converting rotation supported stars into pressure supported stars, a merger with a disk dominated system (and hence negligible supermassive black hole) could grow the bulge more efficiently then the corresponding growth of the black hole by accretion of cold gas (Croton 2006).

As calculated in § 5, in order to satisfy the local scaling relations, assuming that black hole growth is negligible, the stellar mass of the spheroid will have to grow by approximately 60%, while the spheroid mass to light ratio wold have to remain approximately constant, qualitatively consistent with a single dissipative merger (Cox et al. 2006b,a), and associated bursts of star formation. This scenario is similar to that discussed in paper I, to which the reader is referred for further discussion and references, with two important additions: i) the high resolution HST images provide direct evidence for gas rich mergers; ii) our joint analysis of several scaling relations allows us to quantify the expected growth of the spheroid mass and constrain the evolution of the stellar populations of the spheroid via the evolution of the mass-to-light ratio. Our imaging results may also suggest an apparent evolution of Seyfert 1 host galaxy morphologies from $z = 0.36$ to the current epoch. This is because most local Seyfert 1 galaxies have substantial bulges, with normal stellar populations, and no signs of interactions (Hunt et al. 1999). Although currently most Seyfert 1s at z=0 do not show signs of ongoing mergers, they do have hints that these occurred ∼ 1 Gyr earlier (Hunt & Malkan 1999), but that their host galaxy morphologies have settled back down to normal by today (Hunt & Malkan 2004). So our result appears to be consistent with the idea that Seyfert host galaxies, as quiescent galaxies (e.g. Bundy et al. 2004; Lotz et al. 2006), were more disturbed by interactions 4 Gyrs ago than they are today. Unfortunately our sample is too small to make a proper comparison, and to derive statistically significant results. However, we checked the consistency of this statement using the GOODS database. The merger rate for our sample is 3/20 ($0.13^{+0.11}_{-0.07}$) considering only close pairs/mergers, and it increases to 6/20 considering all disturbed systems (0.30 ± 0.12). As a control sample, we selected from GOODS all galaxies with luminosity $17.6 < i' < 20.0$ (i.e. the same range in stellar luminosity that our sample, excluding the point source), in the redshift range $0.26 < z < 0.46$ (morphologies, photometric and spectroscopic redshifts from Bundy et al. 2006) and performed the same visual classification. We found 8/42 close pairs/mergers (0.19 ± 0.07), increasing to 12/42 (0.28 ± 0.08) if we consider all disturbed systems. This is in good agreement with the fraction observed for the distant Seyferts, and somewhat larger than observed in the local universe (e.g. Patton et al. 2002). The small size of our sample does not warrant a more detailed attempt to measure the merger fraction, so this is left for future work and larger samples.

Independent evidence appears to support the scenario discussed above. From the galaxy evolution point of view, although the most massive spheroids appear to have completed most of their growth by $z \sim 1$, it is clear that spheroids of a few 10^{10} $M_{\odot}$ are undergoing significant evolution at $z \sim 0.4$. This view is supported by the signatures of recent star formation detected by Fundamental Plane studies (e.g., Treu et al. 2005b; van der Wel et al. 2005; di Serego Alighieri et al. 2005, and references therein), by the evolution of the mass function (e.g. Bundy, Treu & Ellis 2007 and references therein), and by the evolution of the quenching or

transition mass (e.g., Hopkins et al. 2007, and references therein). From the point of view of black hole demographics, it is hard to pinpoint with sufficient precision the growth of black holes in this mass range, although general arguments based on the global star formation and accretion history suggest that black hole growth may predate bulge growth (e.g., Merloni 2004). At larger masses, the existence of impressively luminous quasars at $z \sim 6$ (Fan et al. 2006) – with the high black hole to host galaxy mass ratio determined by radio observations (Walter et al. 2004), appears to be consistent with our scenario, although it is hard to make a direct comparison, considering that evolution may very well be mass-dependent.

Recent studies of the scaling relations between black hole mass and host galaxy properties tend to focus on higher masses and redshifts than are in our sample. For example, Peng et al. (2006b,a) study the host galaxies of lensed quasars out to $z \sim 4$, ruling out pure luminosity evolution and finding that the ratio between M_{BH} and M_{sph} was ~ 4 times larger at $z \sim 2-3$ than today. Similar results are obtained by other studies of quasar host galaxies at comparable redshifts (Shields et al. 2006; McLure et al. 2006). These results are consistent with our own, although the comparison requires caution considering that the higher redshift studies typically rely on UV broad emission lines and fluxes for estimating M_{BH}, instead of Hβ, and that the contrast between AGN and host light is more unfavorable than in our case. This prevents accurate decomposition of the host spheroid light and direct determination of the stellar velocity dispersion, which needs to be inferred from proxies such as CO and [O III] line widths (Bonning et al. 2005; Salviander et al. 2006; Walter et al. 2004). An alternate approach followed by Adelberger & Steidel (2005) leads to the opposite conclusion. They use the correlation length of AGN hosts at $z \sim 2-3$ to estimate the virial mass of the halo, and the C IV line width and UV flux at 1350Å to estimate M_{BH}. They compare the inferred relation between halo mass and black hole mass with the local relation (Ferrarese 2002), finding no evidence for evolution. Given their error bars, they rule out evolution of over one order of magnitude in the ratio – i.e. evolution of the form $M_{BH}/M_{sph} \propto (1+z)^{2.5}$, with $z \sim 2.5$ – at 90% CL. However, they cannot rule out evolution by a factor of 6 that would be predicted extrapolating our best estimate.

In conclusion, it seems that several lines of evidence are beginning to point in the same direction: black holes appear to complete their growth before their host galaxies. The uncertainties are still large and much work remains to be done before evolution can be considered conclusively detected. However, with the advent of new technologies such as laser guide star adaptive optics and robotic telescopes it will hopefully be possible to improve dramatically our ability to measure black hole masses in the local and distant universe, and thus reduce the main source of error.

7. SUMMARY

This paper is devoted to the study of the cosmic evolution of black holes and their host galaxies. To this aim we have performed a detailed analysis of a sample of 22 Seyfert 1 galaxies at $z \sim 0.36$. The choice of this particular redshift and moderate luminosity AGNs allows us to derive precision measurements of the host galaxy properties, as well as to obtain an estimate of the black hole mass from the dynamics of the broad line region. Using high resolution images taken with ACS we derived luminosity, effective radius and effective surface brightness of the host spheroid as well as nuclear luminosity. We combined this information with emission line widths and stellar velocity dispersion based on high signal to noise Keck spectroscopy (paper I) to construct the M_{BH}-L, M_{BH}-σ and Fundamental Plane relations of distant Seyferts. We compared the $z \sim 0.36$ scaling relations with those followed by local samples of quiescent and active galaxies to determine evolutionary trends. The main results can be summarized as follows:

1. The M_{BH}-L_B relation at $z \sim 0.36$ is inconsistent with the local relation and the assumption of pure luminosity evolution of the host galaxy. Adopting pure luminosity evolution consistent with Fundamental Plane studies, the offset from the local relation corresponds to an offset in present day B-band luminosity of $\Delta \log L_{B,0} = 0.40 \pm 0.11 \pm 0.15$, i.e. $\Delta \log M_{BH} = 0.51 \pm 0.14 \pm 0.19$, in the sense that black holes lived in smaller bulges at $z \sim 0.36$ than today.

2. The M_{BH}-σ relation at $z \sim 0.36$ is inconsistent with the local relation and the assumption of pure luminosity evolution. The offset with respect to the local relation corresponds to $\Delta \log \sigma = 0.13 \pm 0.03 \pm 0.05$, i.e. $\Delta \log M_{BH} = 0.54 \pm 0.12 \pm 0.21$, in the sense that black holes lived in smaller bulges at $z \sim 0.36$ than today.

3. Monte Carlo simulations show that the offset is not the result of selection effects, which are negligible for the M_{BH}-σ relation, and can account for at most 0.1 dex of the observed offset of the M_{BH}-L relation.

4. In order to satisfy the local M_{BH}-σ, M_{BH}-L and FP relations by $z = 0$ – assuming no black hole growth – our distant spheroids have to grow their stellar mass by approximately 60% ($\Delta \log M_{sp} = 0.20 \pm 0.14$) in the next 4 billion years, while preserving their size and holding their stellar mass to light ratio approximately constant. This corresponds to an evolution of the black hole to spheroid mass ratio of the form $M_{BH}/M_{sph} \propto (1+z)^{1.5 \pm 1.0}$.

Assuming that our results are not due to unknown systematic errors or unknown selection effects, the observed evolution can be qualitatively explained if our Seyferts undergo a single collisional merger with a disk-dominated system between z=0.36 and today. This is consistent with the observed merging/interacting fraction and a timescale for merging visibility of ∼1 Gyr. A single merger could increase the spheroid mass by transporting stellar mass from the progenitors disks, without the corresponding growth of the central black holes due to the lack of black hole in the disk dominated system. At the same time, this process would add younger stars to the spheroid (either from the merging disks or from newly formed stars) thus counteracting the fading of the old

stellar populations and producing an approximately constant stellar mass to light ratio in the spheroid. Numerical simulations including realistic prescriptions for star formation, AGN activity and mass loss will be needed to see if these mergers do, indeed, preserve R_e and M_{sph}/L_B. If these indications are supported by future studies, then they will confirm that black holes completed their growth before their host galaxies and are perhaps to be seen less as a by-product of galaxy formation than as an orchestrator (Silk & Rees 1998; Blandford 1999).

We thank David Hogg and the SDSS project for providing calibrated images of the local comparison sample. We thank Aaron Barth, Brad Peterson, Gregory Shields, and Risa Wechsler for discussions. We thank Chien Peng for useful discussions and advice on using galfit and the anonymous referee for useful suggestions and constructive criticism. We are grateful to Kevin Bundy for providing the catalog of galaxies in the GOODS fields with photometric and spectroscopic redshift used to find the control sample described in § 6. This work is based on data obtained with the Hubble Space Telescope and the 10m W.M. Keck Telescope. We acknowledge financial support from NASA through HST grant GO-10216. TT acknowledges support from the NSF through CAREER award NSF-0642621, and from the Sloan Foundation through a Sloan Research Fellowship.

REFERENCES

Adelberger, K. L. & Steidel, C. C. 2005, ApJ, 627, L1
Bentz, M. C., Denney, K. D., Cackett, E. M., Dietrich, M., Fogel, J. K. J., Ghosh, H., Horne, K., Kuehn, C., Minezaki, T., Onken, C. A., Peterson, B. M., Pogge, R. W., Pronik, V. I., Richstone, D. O., Sergeev, S. G., Vestergaard, M., Walker, M. G., & Yoshii, Y. 2006a, ApJ, 651, 775
Bentz, M. C., Peterson, B. M., Pogge, R. W., Vestergaard, M., & Onken, C. A. 2006b, ApJ, 644, 133
Bernardi, M., Sheth, R. K., Tundo, E., & Hyde, J. B. 2006, ArXiv Astrophysics e-prints
Blandford, R. D. 1999, 87
Bonning, E. W., Shields, G. A., Salviander, S., & McLure, R. J. 2005, ApJ, 626, 89
Boylan-Kolchin, M., Ma, C.-P., & Quataert, E. 2006, MNRAS, 369, 1081
Bundy, K., Fukugita, M., Ellis, R. S., Kodama, T., & Conselice, C. J. 2004, ApJ, 601, L123
Bundy, K., et al. 2006, ApJ, 651, 120
Bundy, K., Treu, T., & Ellis, R. S. 2007, ArXiv e-prints, 705, arXiv:0705.1007
Ciotti, L. & Ostriker, J. P. 2007, ArXiv e-prints, arXiv:astro-ph/0703057
Ciotti, L. & van Albada, T. S. 2001, ApJ, 552, L13
Collin, S., Kawaguchi, T., Peterson, B. M. & Vestergaard, M. 2006, A&A, 456, 75
Cox, T. J., Dutta, S. N., Di Matteo, T., Hernquist, L., Hopkins, P. F., Robertson, B., & Springel, V. 2006a, ApJ, 650, 791
Cox, T. J., Jonsson, P., Primack, J. R., & Somerville, R. S. 2006b, MNRAS, 373, 1013
Croton, D. J. 2006, MNRAS, 369, 1808
Croton, D. J., Springel, V., White, S. D. M., De Lucia, G., Frenk, C. S., Gao, L., Jenkins, A., Kauffmann, G., Navarro, J. F., & Yoshida, N. 2006, MNRAS, 365, 11
De Lucia, G. & Blaizot, J. 2007, MNRAS, 375, 2
de Vaucouleurs, G. 1948, Annales d'Astrophysique, 11, 247
Di Matteo, T., Springel, V., & Hernquist, L. 2005, Nature, 433, 604
di Serego Alighieri, S., Vernet, J., Cimatti, A., Lanzoni, B., Cassata, P., Ciotti, L., Daddi, E., Mignoli, M., Pignatelli, E., Pozzetti, L., Renzini, A., Rettura, A., & Zamorani, G. 2005, A&A, 442, 125
Driver, S. P., Allen, P. D., Liske, J., & Graham, A. W. 2007, ApJ, 657, L85
Fan, X., Strauss, M. A., Richards, G. T., Hennawi, J. F., Becker, R. H., White, R. L., Diamond-Stanic, A. M., Donley, J. L., Jiang, L., Kim, J. S., Vestergaard, M., Young, J. E., Gunn, J. E., Lupton, R. H., Knapp, G. R., Schneider, D. P., Brandt, W. N., Bahcall, N. A., Barentine, J. C., Brinkmann, J., Brewington, H. J., Fukugita, M., Harvanek, M., Kleinman, S. J., Krzesinski, J., Long, D., Neilsen, Jr., E. H., Nitta, A., Snedden, S. A., & Voges, W. 2006, AJ, 131, 1203
Ferrarese, L. 2002, ApJ, 578, 90
Ferrarese, L. & Ford, H. 2005, Space Science Reviews, 116, 523
Ferrarese, L. & Merritt, D. 2000, ApJ, 539, L9
Gebhardt, K., Bender, R., Bower, G., Dressler, A., Faber, S. M., Filippenko, A. V., Green, R., Grillmair, C., Ho, L. C., Kormendy, J., Lauer, T. R., Magorrian, J., Pinkney, J., Richstone, D., & Tremaine, S. 2000, ApJ, 539, L13
Gebhardt, K., Lauer, T. R., Kormendy, J., Pinkney, J., Bower, G. A., Green, R., Gull, T., Hutchings, J. B., Kaiser, M. E., Nelson, C. H., Richstone, D., & Weistrop, D. 2001, AJ, 122, 2469
Graham, A. W. & Driver, S. P. 2007, ApJ, 655, 77
Granato, G. L., De Zotti, G., Silva, L., Bressan, A., & Danese, L. 2004, ApJ, 600, 580
Greene, J. E. & Ho, L. C. 2006, ApJ, 641, L21
Greene, J. E. & Ho, L. C. 2007, ArXiv Astrophysics e-prints, 705, arXiv:0705.0020
Haehnelt, M. G. & Kauffmann, G. 2000, MNRAS, 318, L35
Häring, N. & Rix, H.-W. 2004, ApJ, 604, L89
Hopkins, P. F., Bundy, K., Hernquist, L., & Ellis, R. S. 2007, ApJ, 659, 976
Hopkins, P. F., Hernquist, L., Cox, T. J., Di Matteo, T., Robertson, B., & Springel, V. 2006b, ApJS, 163, 1
Hopkins, P. F., Hernquist, L., Cox, T. J., Robertson, B., & Krause, E. 2007, ArXiv Astrophysics e-prints
Hunt, L. K. & Malkan, M. A. 1999, ApJ, 516, 660
—. 2004, ApJ, 616, 707
Hunt, L. K., Malkan, M. A., Moriondo, G., & Salvati, M. 1999, ApJ, 510, 637
Kaspi, S., Maoz, D., Netzer, H., Peterson, B. M., Vestergaard, M., & Jannuzi, B. T. 2005, ApJ, 629, 61
Kaspi, S., Smith, P. S., Netzer, H., Maoz, D., Jannuzi, B. T., & Giveon, U. 2000, ApJ, 533, 631
Kormendy, J. & Richstone, D. 1995, ARA&A, 33, 581
Lotz, J. M., Davis, M., Faber, S. M., Guhathakurta, P., Gwyn, S., Huang, J., Koo, D. C., Le Floc'h, E., Lin, L., Newman, J., Noeske, K., Papovich, C., Willmer, C. N. A., Coil, A., Conselice, C. J., Cooper, M., Hopkins, A. M., Metevier, A., Primack, J., Rieke, G., & Weiner, B. J. 2006, ArXiv Astrophysics e-prints
Magorrian, J., Tremaine, S., Richstone, D., Bender, R., Bower, G., Dressler, A., Faber, S. M., Gebhardt, K., Green, R., Grillmair, C., Kormendy, J., & Lauer, T. 1998, AJ, 115, 2285
Malbon, R. K., Baugh, C. M., Frenk, C. S., & Lacey, C. G. 2006, ArXiv Astrophysics e-prints, astro-ph/0607424
Marconi, A. & Hunt, L. K. 2003, ApJ, 589, L21
McLure, R. J., Jarvis, M. J., Targett, T. A., Dunlop, J. S., & Best, P. N. 2006, MNRAS, 368, 1395
Merloni, A. 2004, MNRAS, 353, 1035
Miralda-Escudé, J. & Kollmeier, J. A. 2005, ApJ, 619, 30
Netzer, H. & Trakhtenbrot, B. 2007, ApJ, 654, 754
Nipoti, C., Londrillo, P., & Ciotti, L. 2003, MNRAS, 342, 501
Novak, G. S., Faber, S. M., & Dekel, A. 2006, ApJ, 637, 96
Onken, C. A., Ferrarese, L., Merritt, D., Peterson, B. M., Pogge, R. W., Vestergaard, M., & Wandel, A. 2004, ApJ, 615, 645
Patton, D. R., Pritchet, C. J., Carlberg, R. G., Marzke, R. O., Yee, H. K. C., Hall, P. B., Lin, H., Morris, S. L., Sawicki, M., Shepherd, C. W., & Wirth, G. D. 2002, ApJ, 565, 208
Peng, C. Y., Ho, L. C., Impey, C. D., & Rix, H.-W. 2002, AJ, 124, 266
Peng, C. Y., Impey, C. D., Ho, L. C., Barton, E. J., & Rix, H.-W. 2006a, ApJ, 640, 114
Peng, C. Y., Impey, C. D., Rix, H.-W., Kochanek, C. S., Keeton, C. R., Falco, E. E., Lehár, J., & McLeod, B. A. 2006b, ApJ, 649, 616
Peterson, B. M. 2007, ArXiv Astrophysics e-prints

Peterson, B. M., Ferrarese, L., Gilbert, K. M., Kaspi, S., Malkan, M. A., Maoz, D., Merritt, D., Netzer, H., Onken, C. A., Pogge, R. W., Vestergaard, M., & Wandel, A. 2004, ApJ, 613, 682
Robertson, B., Hernquist, L., Cox, T. J., Di Matteo, T., Hopkins, P. F., Martini, P., & Springel, V. 2006, ApJ, 641, 90
Salviander, S., Shields, G. A., Gebhardt, K., & Bonning, E. W. 2006, ApJ, in press, astro-ph/0612568
Sersic, J. L. 1968
Sheth, R. K., Bernardi, M., Schechter, P. L., Burles, S., Eisenstein, D. J., Finkbeiner, D. P., Frieman, J., Lupton, R. H., Schlegel, D. J., Subbarao, M., Shimasaku, K., Bahcall, N. A., Brinkmann, J., & Ivezić, Ž. 2003, ApJ, 594, 225
Shields, G. A., Gebhardt, K., Salviander, S., Wills, B. J., Xie, B., Brotherton, M. S., Yuan, J., & Dietrich, M. 2003, ApJ, 583, 124
Shields, G. A., Menezes, K. L., Massart, C. A., & Vanden Bout, P. 2006, ApJ, 641, 683
Silk, J. & Rees, M. J. 1998, A&A, 331, L1
Tremaine, S., Gebhardt, K., Bender, R., Bower, G., Dressler, A., Faber, S. M., Filippenko, A. V., Green, R., Grillmair, C., Ho, L. C., Kormendy, J., Lauer, T. R., Magorrian, J., Pinkney, J., & Richstone, D. 2002, ApJ, 574, 740
Treu, T., Ellis, R. S., Liao, T. X., & van Dokkum, P. G. 2005a, ApJ, 622, L5
Treu, T., Ellis, R. S., Liao, T. X., van Dokkum, P. G., Tozzi, P., Coil, A., Newman, J., Cooper, M. C., & Davis, M. 2005b, ApJ, 633, 174
Treu, T., Malkan, M. A., & Blandford, R. D. 2004, ApJ, 615, L97
Treu, T., Stiavelli, M., Bertin, G., Casertano, S., & Møller, P. 2001a, MNRAS, 326, 237
Treu, T., Stiavelli, M., Møller, P., Casertano, S., & Bertin, G. 2001b, MNRAS, 326, 221
van der Wel, A., Franx, M., van Dokkum, P. G., Rix, H.-W., Illingworth, G. D., & Rosati, P. 2005, ApJ, 631, 145
Vestergaard, M. 2002, ApJ, 571, 733
Vestergaard, M. & Peterson, B. M. 2006, ApJ, 641, 689
Walter, F., Carilli, C., Bertoldi, F., Menten, K., Cox, P., Lo, K. Y., Fan, X., & Strauss, M. A. 2004, ApJ, 615, L17
Wandel, A., Peterson, B. M., & Malkan, M. A. 1999, ApJ, 526, 579
Woo, J.-H., Treu, T., Malkan, M. A., Ferry, M. A., & Misch, T. 2007, ApJ, 661, 60
Woo, J.-H., Treu, T., Malkan, M. A., & Blandford, R. D. 2006, ApJ, 645, 900
Woo, J.-H., Urry, C. M., Lira, P., van der Marel, R. P., & Maza, J. 2004, ApJ, 617, 903
Woo, J.-H., Urry, C. M., van der Marel, R. P., Lira, P., & Maza, J. 2005, ApJ, 631, 762

TABLE 1
Sample properties

Name (1)	RA (J2000) (2)	DEC (J2000) (3)	z (4)	i' (5)	σ (6)
S01	15 39 16.23	+03 23 22.06	0.3596	18.74	132 ± 8
S02	16 11 11.67	+51 31 31.12	0.3544[a]	18.94	-
S03	17 32 03.11	+61 17 51.96	0.3583[a]	18.20	-
S04	21 02 11.51	-06 46 45.03	0.3580	18.41	186± 8
S05	21 04 51.85	-07 12 09.45	0.3531	18.35	132± 5
S06	21 20 34.19	-06 41 22.24	0.3689	18.41	169±14
S07	23 09 46.14	+00 00 48.91	0.3520	18.11	145±13
S08	23 59 53.44	-09 36 55.53	0.3591	18.42	187±11
S09	00 59 16.11	+15 38 16.08	0.3548	18.16	187±15
S10	01 01 12.07	-09 45 00.76	0.3506[a]	17.92	-
S11	01 07 15.97	-08 34 29.40	0.3562	18.34	127± 9
S12	02 13 40.60	+13 47 56.06	0.3575	18.12	173±22
S16	11 19 37.58	+00 56 20.42	0.3702[a]	19.22	-
S21	11 05 56.18	+03 12 43.26	0.3534[a]	17.21	-
S23	14 00 16.66	-01 08 22.19	0.3515	18.08	172± 8
S24	14 00 34.71	+00 47 33.48	0.3621	18.21	214±10
S26	15 29 22.26	+59 28 54.56	0.3691	18.88	128± 8
S27	15 36 51.28	+54 14 42.71	0.3667[a]	18.80	-
S28	16 11 56.30	+45 16 11.04	0.3682	18.59	210±10
S29	21 58 41.93	-01 15 00.33	0.3575[a]	18.77	-
S31	10 15 27.26	+62 59 11.51	0.3504[a]	18.14	-
S99	16 00 02.80	+41 30 27.00	0.3690	18.33	224±12

Note. — Col. (1): Target ID. Col. (2): RA. Col. (3): DEC. Col. (4): Redshift from stellar absorption lines. Col. (5): Extinction corrected i' AB magnitude from SDSS photometry. Col. (6): Stellar velocity dispersion in kms^{-1} from paper I.
[a] redshift from SDSS DR4.

TABLE 2
New measurements

Name (1)	i' (total) (2)	i' (spheroid) (3)	$\log L_{\mathrm{B}}/L_{\odot,\mathrm{B}}$ (4)	$\mathrm{SB_{e,B}}$ (5)	$\mathrm{R_e}$ (6)	$\mathrm{L_{5100}}$ (7)	$\mathrm{f_{nuc}}$ (8)	$\log M_{\mathrm{BH}}/M_{\odot}$ (9)
S01	18.50	19.92	10.28	21.85	5.29	0.74	0.29	8.21
S02	19.03	19.85	10.31	20.27	2.63	0.36	0.22	7.99
S03[a]	17.94	20.23	10.16	17.04	0.50	1.69	0.39	8.29
S04	18.06	20.12	10.20	18.36	0.96	1.42	0.36	8.45
S05	17.93	20.45	10.07	18.84	1.03	2.04	0.47	8.77
S06	18.35	20.48	10.06	18.81	1.01	0.54	0.18	8.17
S07	17.79	20.35	10.11	18.69	1.01	2.26	0.45	8.55
S08	18.31	21.75	9.55	20.50	1.23	1.25	0.40	8.10
S09	18.17	19.00	10.65	19.87	3.24	0.78	0.22	8.15
S10[a]	18.01	19.30	10.53	16.08	0.49	1.11	0.27	8.27
S12[a]	18.12	21.16	9.78	18.14	0.54	1.05	0.28	8.69
S16	19.14	22.26	9.34	19.97	0.76	0.70	0.48	8.26
S21[a]	17.45	18.95	10.67	15.82	0.51	2.30	0.34	8.81
S23[a]	17.99	20.85	9.91	17.93	0.57	1.20	0.29	8.72
S24	18.06	18.59	10.81	22.41	12.6	0.44	0.11	8.33
S26	18.87	20.06	10.23	17.73	0.75	0.50	0.27	8.01
S27	18.51	19.46	10.46	21.17	4.78	0.92	0.36	8.10

Note. — Col. (1): Target ID. Col. (2): Total extinction corrected F775W AB magnitude. Col. (3): Spheroid extinction corrected F775W AB magnitude. Col. (4): $\mathrm{Log_{10}}$ of spheroid luminosity in rest frame B (solar units), not corrected for evolution. Errors are estimated to be 0.2 dex. Col. (5): Spheroid effective surface brightness in rest frame B (AB magnitudes arcsec^{-2}; see § 2.2.2 for error discussion). Col. (6): Spheroid effective radius (kpc; see § 2.2.2 for error discussion). Col. (7): Nuclear luminosity at 5100 Å (10^{44} erg s^{-1}). Errors are estimated to be 20%. Col. (8): Nuclear light fraction in F775W. Errors are estimated to be 20%. Col. (9): $\mathrm{Log_{10}}$ of $\mathrm{M_{BH}}$ (solar units). Random errors are estimated to be 0.4 dex. Systematic errors are discussed extensively in Section 4
[a] Spheroid size and luminosity are upper limits.

TABLE 3
PROPERTIES OF THE LOCAL COMPARISON SAMPLE.

Name (1)	z (2)	$\log L_B/L_{\odot,B}$ (3)	$\log M_{BH}/M_\odot$ (4)
Ark120	0.032	10.82	8.18
Mrk79	0.022	9.79	7.72
Mrk110	0.035	9.85	7.40
Mrk590	0.026	10.40	7.68
Mrk817	0.031	10.49	7.69
NGC3227	0.004	8.85	7.62
NGC4051	0.002	8.43	6.28
NGC4151	0.003	9.49	7.66
NGC5548	0.017	10.53	7.83

NOTE. — Col. (1): Target ID. Col. (2): Redshift. Col. (3): Log_{10} of spheroid Luminosity in rest frame B (solar units). Col. (4): Log_{10} of M_{BH} (solar units). From (Peterson et al. 2004) and (Bentz et al. 2006b). Errors are estimated to be 0.4 dex.